# Application of parametric statistical analysis to processing data of a micro-pulse aerosol lidar

**I.A. Razenkov, H.K. Cha,* D.H. Kim,* N.A. Shefer**

*Institute of Atmospheric Optics,*
*Siberian Branch of the Russian Academy of Sciences, Tomsk, Russia*
** Korean Institute of Atomic Energy, Tajon, South Korea*

Received April 6, 2000

Using an array of sensing data obtained with a micro-pulse aerosol lidar data as an example, two spectral statistical methods of data processing are compared. The methods compared are the non-parametric method that uses a fast Fourier transform (FFT) and the parametric one based on a model of "autoregression moving average" (ARMA). The calculations have been carried out following the two-channel spectral estimation scheme by the Nuttall–Strand method for the ARMA model. Spatiotemporal distributions of the coherency and phase spectra were calculated from spatiotemporal distribution of atmospheric aerosol scattering coefficient. The advantages of parametric approach ensuring more high frequency resolution and higher accuracy of obtained spectral estimates are shown. At interpretation of aerosol lidar data, the coherency spectrum was indicative of the regions in space, where temperature inversion could happen. The phase spectrum makes it possible to detect zones in the troposphere of slowly ascending and descending aerosol inhomogeneities. It is proposed to start spectral processing of lidar data with the ARMA model of the second order to obtain smoothed spectral estimates.

## Introduction

The use of correlation or spectral analysis in processing data of lidar sensing makes it possible to essentially increase the bulk of information that may thus be extracted. The idea of statistically processing lidar data is not new. Eloranta[1] and other researchers[2,3] successfully applied classical, or non-parametric, approach based on the fast Fourier transform to estimating the wind velocity, spectra of atmospheric turbulence, the rate of dissipation of kinetic energy, and so on. The accuracy of statistical estimates obtained by a non-parametric approach and their frequency resolution depend on the sample length.[4,5]

One of the principal peculiarities of the processes occurring in the atmosphere is a very wide spectrum of the scales of physical parameters such as wind velocity, temperature, pressure, aerosol number density, etc. The spectra of these parameters range from millimeters to hundreds and thousands of kilometers.[6] Besides, the low-frequency fluctuations cause unsteady-state (trends) behavior of high-frequency components of the process observed, and one should give due regard to this fact in the corresponding analysis.

In observing slow low-frequency mesoscale processes, researchers face the problem on acquiring the bulk of initial data, which would suffice analysis to be carried out. Let us show this by an example. Let us suppose that one needs to obtain a power spectrum of fluctuations of an atmospheric parameter in the troposphere in the range of spatial scales from 1 to 100 km. Let us assume that the mean wind at a given altitude is 10 m/s. Then, according to Kotelnikov theorem, the duration of observations (Nyquist frequency)[4] should be no less than $2 \times 1000$ m/10 m/s $\approx$ 3 min. One should choose the total duration of an observation to be on the order of $10 \times 100000$ m/10 m/s $\approx$ 30 hours, if it is planned to record at least 10 inhomogeneities of a 100-km size. If the frequency resolution of 0.333 cycle/hour has been chosen that corresponds to the size of 100 km, then the error in estimating the spectrum is 22%.[6] Of course, one can decrease the error by lowering the frequency resolution or due longer observations which is quite long and exceeds one day.

Let us note that an increase in the duration of observations can have no positive effect if the process under study is an unsteady-state one. It happens so that most interesting atmospheric situations such as during the passage of atmospheric fronts are the unsteady-state ones and relatively transient. For example, the characteristic size of frontal zones at the boundaries of air masses is of 50 to 100 km, and the time of front passage through an observation point is a few hours.[7]

This was the reason why we have turned our attention to the parametric approach[8] to spectral estimation of short data series. The parametric statistics enables one to obtain the spectra with a higher resolution than the classical non-parametric approach.[5] A short data series is defined as a series of data for which the obtained spectral resolution has the same order as the value inverse to the length of this series. In other words, the parametric spectrum provides for data on variations, the period of which is comparable with the length of the sample.

This is a very important fact because the non-parametric approach requires the trends to be removed by means of, for example, power polynomials[4] before Fourier analysis. Let us remind that a trend is defined as a low-frequency component of the process, the period

0235-6880/00/10 865-09 $02.00 

of which is comparable with the length of the sample. Otherwise, the spectral estimates will suffer an additional error. In analyzing parametrically, it is sufficient to remove only linear trend, i.e., the variations with the period many times greater than the sample length.[8]

Hence, application of the parametric approach makes it possible to transform the low-frequency variations of the process from disturbing factor to useful information. Moreover, the low-frequency fluctuations can be of interest for researchers.

The purpose of this paper is to experimentally examine the parametric way of processing samples of short data series on aerosol acquired with a micro-lidar and to obtain additional information about the processes occurring in the atmosphere.

## Method

Parametric description of the statistics of second order is based on the model of time series corresponding to the random process to be analyzed. We investigated models[8] of a class of processes initiated by a white noise, that possess the rational system functions. The model of an autoregression moving average (ARMA) process was chosen from this class. The output processes of the models of this class have spectral power density, which can completely be described using the parameters of the model and variance of a white noise like process.[8] Some information is often available in practice about the process, from which the data have been read. This information can be used for construction of the model approximating the process, which produced the observed time series.

The parametric method of spectral estimations involves three stages. The parametric model of a time series corresponding to the available record of the measurement data is being chosen at the first stage. The ARMA model of the time series appropriate for approximation of many stochastic processes with discrete time is described by the output of a digital filter with the complex coefficients

$$x[n] = -\sum_{k=1}^{p} A[k]\, x[n-k] + \sum_{k=0}^{p} B[k]\, u[n-k], \quad (1)$$

where $u[k]$ is the input sequence, $x[n]$ is the sequence at the filter output, and $p$ is the order of the model.

We have selected a mixed ARMA model for two reasons. First, theoretical spectrum of fluctuations of the atmospheric parameters is smooth without any sharp depressions,[9] which is often called the Kolmogorov one. The moving average model corresponds to such a spectrum.[8] Second, the autoregression can satisfactorily describe sharp increases and decreases in the spectrum, for example, when a sample contains variations in a narrow frequency range.[8] Such situations can occur in the atmosphere under conditions of stable thermal stratification[10] when the appearance of flotation waves is possible. Let us note that at present choosing models for parametric spectral estimation is practically limited to the aforementioned three models.

The multi-channel ARMA models are most informative at laser sounding of the atmosphere. The multi-channel analysis of time series makes it possible to simultaneously process the data from several channels and to estimate their interrelations. The output $x[n]$ and initiating $u[k]$ processes in Eq. (1) are transformed in the case of $M$-channel ARMA process to the $M \times 1$ vectors, and the coefficients $A[k]$ and $B[k]$ are replaced by the $M \times M$ matrices of autoregression parameters.[8]

The estimates of the model parameters are calculated at the second stage, i.e., the matrices of the coefficients $A[k]$ and $B[k]$. In so doing, we used the Nuttall–Strand method, which is the multi-channel version of the harmonic average.[8] This method is based on estimating the cross correlation coefficient. The Nuttall–Strand method is described in detail in Refs. 11 and 12.

At the third stage, the values of the estimated parameters are substituted into a theoretical formula describing spectral power density corresponding to the model chosen. The estimation obtained is the auto-spectra $G_{xx}(f)$ and cross-spectra $G_{xy}(f)$, which will be considered below. All the calculated spectra are discrete, but, for simplicity, we denote them as functions of frequency in parentheses.

The auto-spectrum, or merely spectrum, is a series expansion of the variance of the process over frequency. Indices "$xx$" indicate the process (or time series) $x(t)$ which is denoted in discrete representation as $x[n]$. If the time interval between the neighboring readouts is $\Delta t$, then $x(t) = x(n\Delta t) = x[n]$. The maximum of the spectrum $G_{xx}(f_{\max})$ shows oscillations or fluctuations of what power and at which frequency dominate in the sample $x[n]$.

The mutual, or cross-spectrum $G_{xy}(f)$ is a complex quantity, and therefore it is inconvenient to consider it in a usual form. Indices "$xy$" indicate the time series $x(t)$ and $y(t)$. Usually the cross-spectrum $G_{xy}(f)$ is presented in the form of two real functions of frequency[4]: the coherency spectrum $\gamma^2_{xy}(f)$ and the phase spectrum $\theta_{xy}(f)$, which we shall call the "coherency" and "phase" spectrum, respectively.

The coherency spectrum $\gamma^2_{xy}(f)$ is defined as

$$\gamma^2_{xy}(f) = |G_{xy}(f)|^2 / [G_{xx}(f)\, G_{yy}(f)], \quad (2)$$

where $G_{xx}(f)$ and $G_{yy}(f)$ are the auto-spectra of the time series $x(t)$ and $y(t)$, respectively. The coherency spectrum (2) is dimensionless and varies from 0 to 1, indicating, what a fraction of the process $y(t)$ is caused by linear transformation of the process $x(t)$ at the frequency $f$.

Let us explain the meaning of the coherency spectrum $\gamma^2_{xy}(f)$. Let, for example, $x(t)$ and $y(t)$ be related to each other by a linear dependence

$y(t) = ax(t) + b$, where $a$ and $b$ are constants, then the coherency spectrum $\gamma^2_{xy}(f) \equiv 1$. If the processes $x(t)$ and $y(t)$ are not related to each other, i.e., their sources are different, then $\gamma^2_{xy}(f) \equiv 0$. If $y(t) = ax(t) + z(t)$, where $z(t)$ is an independent process, for example, noise, then $0 < \gamma^2(f) < 1$. This is schematically illustrated in Fig. 1, in which the rectangles show the neighbor aerosol layers. The number of arrows between the layers indicates the degree of statistical correlation between the layers.

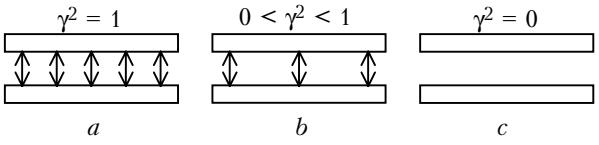


**Fig. 1.** Three variants of the statistical interaction of the neighboring aerosol layers explaining the meaning of the coherency spectrum: strong interaction (*a*), intermediate case (*b*); and no interaction (*c*).

The phase spectrum (or "phase") $\theta_{xy}(f)$ is defined by the cross-spectrum $G_{xy}(f)$ as

$$\theta_{xy}(f) = \arctan [\mathrm{Im}\, G_{xy}(f) / \mathrm{Re}\, G_{xy}(f)]. \qquad (3)$$

Equation (3) allows one to calculate the phase angle at the frequency $f$ between the processes $x(t)$ and $y(t)$, which is proportional to the time delay between these processes.[4,5] For example, theoretical formula for the phase spectrum[5] $\theta_{xy}(f)$ when the process $y(t)$ is behind $x(t)$ by the time $\tau$, i.e., $y(t) = x(t - \tau)$, has the form

$$\theta_{xy}(f) = -2\pi f\tau. \qquad (4)$$

In principle, the phase makes it possible to estimate the modulus and direction of the velocity of a slow motion of the aerosol inhomogeneities along the vertical direction, however, the accuracy is low when sounding in only vertical direction.[13] Nevertheless, the phase can be used for qualitative analysis to determine the direction of propagation of the aerosol inhomogeneities along the vertical direction. If, when calculating the phase, the first time series has corresponded to higher altitude than the second one, it follows from (4) that the phase should be negative at motion of the aerosol inhomogeneities downwards. Respectively, the phase is positive at the upgoing motion of the inhomogeneities.

## Procedure of calculation and experiment

Now let us define, in which form one can use the coherency, $\gamma^2_{xy}(f)$, and phase, $\theta_{xy}(f)$, spectra when interpreting the data of laser sounding of the aerosol density. Let the processes $x(t)$ and $y(t)$ introduced above be a time series of observations over aerosol scattering coefficient $\sigma(z, t)$ at two altitudes $z_1$ and $z_2$, i.e.,

$$x(t) = \sigma(z_2 = z_1 + \Delta z,\ t_1 + t);$$
$$y(t) = \sigma(z_1,\ t_1 + t), \qquad (5)$$

where $t_1$ is the fixed moment in time, $\Delta z$ is the height resolution of lidar measurements. The parameters $z_1$ and $t_1$ included into the formula show that different parts of the data array can be spectrally processed.

It follows from Eq. (5) that $z_2 = z_1 + \Delta z$, so the coherency spectrum (2) will show the strength of the statistically linear relation of the aerosol densities at the neighbor heights $z_1$ and $z_1 + \Delta z$, which we will denote as $\gamma^2(z_1, t_1, f)$. To better estimate $\gamma^2(z_1, t_1, f)$, it is desirable to average the coherency spectrum at the neighbor heights. Let $N_z$ be the number of averaging acts over height, and $N_t$ the number of points in the time series at spectral estimations. Then, changing the height $z_1$ and time $t_1$, one can obtain information about the coherency spectrum $\gamma^2(z_1, t_1, f)$ with the spatial resolution along the vertical direction $\Delta z\, N_z$ and temporal resolution $\Delta t\, N_t$.

When interpreting the data of laser sounding of atmospheric aerosol, the approach applied to estimating the phase spectrum $\theta(z_1, t_1, f)$ was identical to that of estimating the coherency spectrum mentioned above.

The experiment was carried out using the aerosol laser radar set similar to the system described in Ref. 14. Such lidars are often called micro-pulse lidars (MPL). The MPL-systems contain low-power diode-pumped solid-state (DPSS) lasers. However, high repetition rate of sounding pulses and counting mode of operation of a PMT makes it possible to carry out sounding of aerosol up to the height of 10 km and higher. A MPL-lidar is capable of operating in automated mode for a long time.

Sounding was carried out along vertical direction. Spatial resolution of the lidar measurements was 100 m. The lidar data were accumulated during 2–3 minutes and so the discretization frequency was 20–30 cycles/hour. Total time of the data accumulation could be 12 hours and longer. Each lidar return profile was recalculated to the total scattering coefficient using Klett's method.[15] As a result, by the end of each series of observations, we had gotten a spatiotemporal distribution of the aerosol scattering coefficient.

The scheme of calculations of the spectral characteristics is shown in Fig. 2. First, the parameters were selected: the number of points $N_t$ and the number of pairs of series for averaging $N_z$, intervals of time $\Delta t$ and height $\Delta z$; the method for calculation and the order of the ARMA model $p$. Then the time series were formed for the fixed values of height $z_1$ and time $t_1$, from which the trend was removed[4]: linear for the ARMA model and polynomial of the 5th power for the FFT. Then the matrices of coefficients $A[k]$ and $B[k]$ were calculated for the ARMA model. At the next stage the auto- and cross-spectra were calculated as well as the coherency and phase spectra with the prescribed frequency resolution.

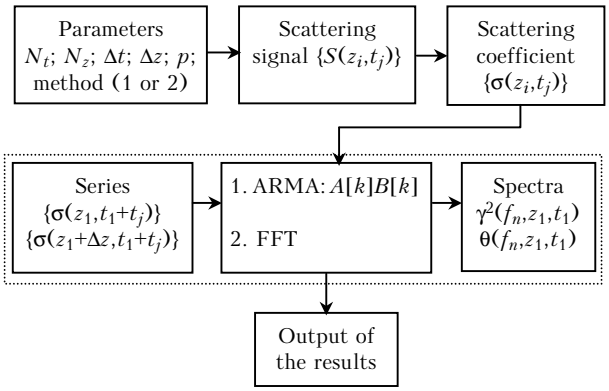


**Fig. 2.** Scheme of calculation of the spectral functions from the lidar data.

The described scheme for calculation was repeated many times for all heights by means of changing the height $z_1 = z_1 + \Delta z$ and time moment $t_1 = t_1 + \Delta t_1$. The value $\Delta t_1 = N_t \Delta t/4$ that means 25% overlap of the neighbor data, because time averaging was $N_t \Delta t$. Averaging over height was performed over $N_z$ spectra. When displacing along the height, overlap of the neighbor data was 50%, i.e., displacing along the height was $N_z \Delta z/2$ after each averaging in the layer of the thickness $N_z \Delta z$. In the end, the results obtained were displayed in one or another form, but usually it was 2D mapping.

An example of the initial data in the form of gray-scale pictures showing the spatiotemporal maps of the scattering coefficient is shown in Fig. 3. The gray scale is logarithmic. The scattering coefficient is represented in reciprocal kilometers. Sounding was performed in Tajon (South Korea) on the night 20 to 21 of November, 1998. Time resolution was $\Delta t$ = 3 min, and height resolution was $\Delta z$ = 100 m. The situation shown in Fig. 3 is interesting by the fact that cold air mass passed over the observation site. Low-layer cloudiness appeared after 1 a.m. at the height of 2.5 km, which then slowly descended.

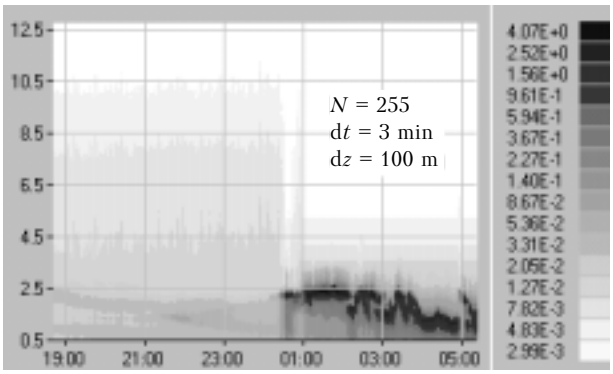


**Fig. 3.** Spatiotemporal distribution of the aerosol scattering coefficient obtained by means of the MPL lidar on November 20–21, 1998 in Tajon, Korea.

## Results

All results presented here have been obtained from the data shown in Fig. 3. The main parameter of the ARMA model, which was changed in calculations, was the order of the ARMA model. All calculations were performed for $N_t$ = 32 and $N_z$ = 10.

Figure 4 shows the time series (*a*) of the scattering coefficient since 10 p.m. until 11:30 p.m. at the heights of 900 and 1000 m, and the corresponding auto-spectra (*b*), coherency (*c*), and phase (*d*) spectra.

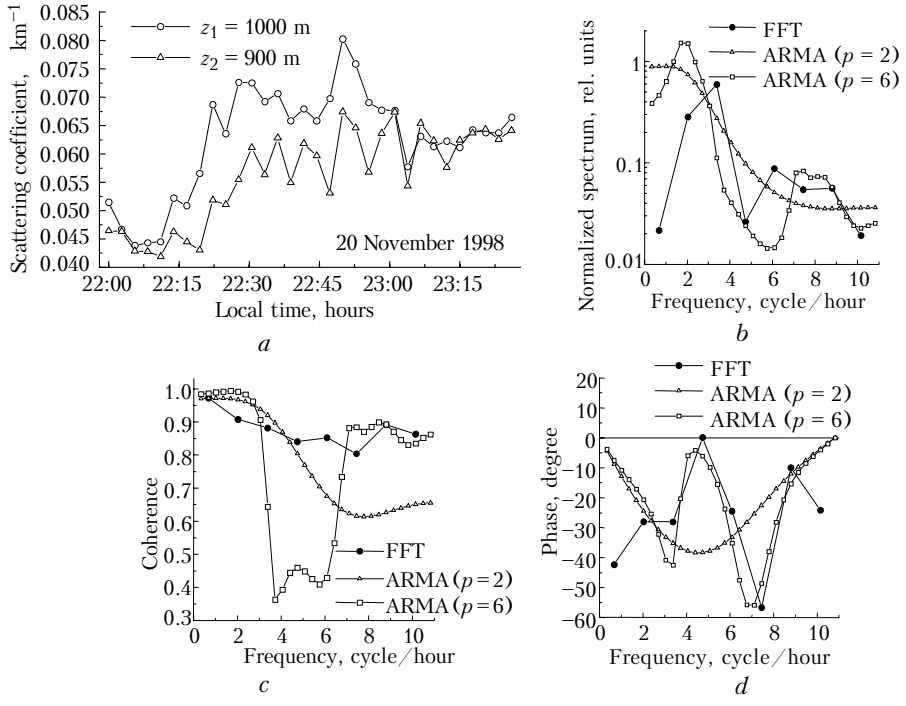


**Fig. 4.** Time series (*a*) and corresponding power (*b*), coherence (*c*), and phase (*d*) spectra.

Three curves are shown in Figs. 4*b*, *c*, and *d*. The first curve (circles) corresponds to the spectra calculated by classic method using FFT.[4] Two other spectra were obtained by ARMA method for $p = 2$ (triangles) and $p = 6$ (squares). Frequency resolution of the ARMA method was selected four times higher than the classic approach allowed. Figure 4 clearly illustrates the possibilities of the parametric estimation of the spectra. The higher frequency resolution and greater stability of the obtained spectral estimates are an evidence of this fact.

Comparison of the non-parametric and parametric methods was carried out as follows. Coherency and phase spectra were calculated for three values of the frequency by FFT and ARMA methods at $p = 2$. The frequency values were selected in the low-frequency range ($f = 1$ cycle/hour), in the middle of the range ($f = 5$ cycle/hour) and in the high-frequency range ($f = 10$ cycle/hour). The result was displayed in the form of spatiotemporal maps analogous to Fig. 3. Temporal resolution of the spectral maps was about 1.5 hours, and the spatial resolution was 1 km. The maps were filled by the method of linear interpolation.

Six spatiotemporal maps of the coherency spectra calculated based on the data shown in Fig. 3 are shown in Fig. 5. The coherency spectrum obtained by non-parametric method using the FFT technique for three values of frequency $f = 1$, 5, and 10 cycle/hour is shown in Figs. 5*a*, *c*, and *e*.

The coherency spectra calculated using the non-parametric approach for the ARMA model, $p = 2$, for the same frequencies are shown in Figs. 5*b*, *d*, and *f*. Figure 5 shows that the coherency spectra for the ARMA model have more regular monotonic structure in time and space than the FFT spectra. It also follows from Fig. 5 that a regular process occurred in the tropospheric layer. The coherence took values below 0.5 that is presented by a light colored stripe. We will discuss it in detail below.

Six spatiotemporal maps of the phase spectra calculated based on the data shown in Fig. 3 are presented in Fig. 6. The phase obtained by non-parametric method using the FFT method for three values of frequency $f = 1$, 5, and 10 cycle/hour is shown in Figs. 6*a*, *c*, and *e*. The phase spectra calculated using the non-parametric approach for the ARMA model, $p = 2$, for the same frequencies are shown in Figs. 6*b*, *d*, and *f*. Figure 6 shows that the phase spectra for the ARMA model have more regular monotonic structure in time and space than the FFT spectra.

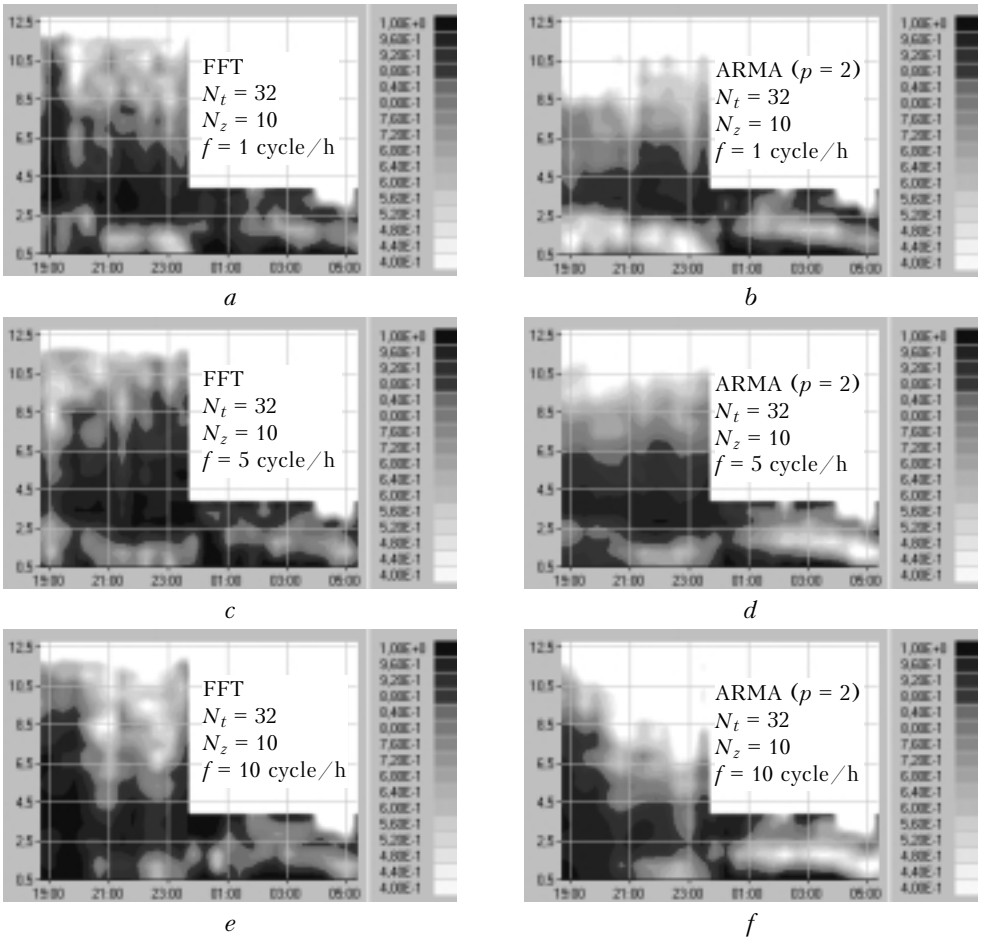


**Fig. 5.** Spatiotemporal maps of the coherence spectra calculated by means of FFT (*a*, *c*, *e*) and the ARMA method at $p = 2$ (*b*, *d*, *f*).

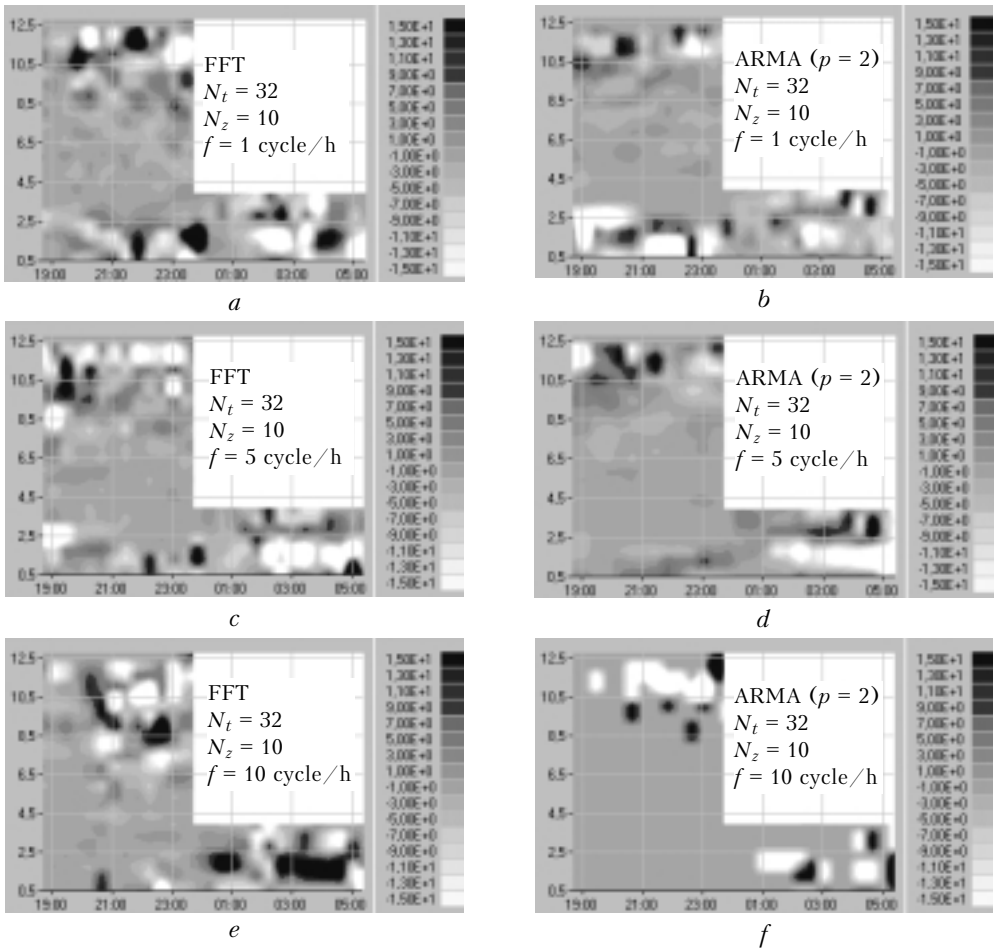


**Fig. 6.** Spatiotemporal maps of the phase spectra calculated by means of FFT (*a*, *c*, *e*) and the ARMA method at $p = 2$ (*b*, *d*, *f*).

The most monotonic is the map (Fig. 6*d*) obtained for the ARMA model at $f = 5$ cycle/hour. It is quite regular, because the phase value is small at low frequencies that follows from Eq. (4). The phase can be "broken" at high frequencies for different reasons: jumps through zero, low signal-to-noise ratio, and so on. Comparison of analogous phase spectra in Figs. 6*c* and *d* for FFT and ARMA methods is also in favor of the parametric approach. The characteristic ranges are observed in the tropospheric layer in Fig. 6*d*, where the phase was first positive, and then negative. An explanation of such a behavior will be given below.

Comparison of the calculated results obtained at different values of the order of the model $p$ is shown in Fig. 7, where the coherency (*a*, *c*, *e*) and phase (*b*, *d*, *f*) spectra are shown for the ARMA method with the values of the model $p = 2$, 6, and 10. It is seen from Fig. 7 that the high-frequency components become more pronounced as the order of the ARMA model increases. It is clear that the order of the model $p$ should be chosen depending on the problem to be solved. It is important to keep in mind that the spectral estimates obtained at small $p$ values are smoother. In our opinion, it is always better to start analysis of the lidar data with low $p$ values, in order to obtain good idea on the situation as a whole, excluding fine details.

According to this principle, let us consider in a more detail the calculated results on the coherency and phase spectra obtained by the ARMA method for $p = 2$ from the same data on November 20–21, 1998. Let us concentrate on the lower troposphere in the layer from 0.5 up to 3.5 km. Figure 8 shows the maps of the aerosol scattering coefficient (*a*) and coherency (*b*) and phase (*c*, *d*) spectra calculated based on it by ARMA method. Two maps of positive (Fig. 8*c*) and negative (Fig. 8*d*) values of phase are drawn for more clear representation is black-and-white mode. This made it possible to distinctly isolate the region of the positive phase values, i.e., the region where the aerosol inhomogeneities moved upwards. As it follows from Fig. 8*c*, it was observed since 8 p.m. until 1 a.m. The height of the region of positive phase ascended from below up to the height of 2 km.

Analogously, it follows from Fig. 8*d* that after 1 a.m. the aerosol inhomogeneities began to move downwards, because the phase is negative. The region of downward motion descended from the height of 2 km since 1 a.m. until 5:30 a.m. The regions of up and downward motion are shown in Fig. 8 by straight lines.

Let us give some physical explanations of the results obtained. Diurnal behavior of air temperature on

20–21 November 1998 near ground at the observation site is shown in Fig. 9. It follows from Fig. 9 that the invasion of the cold air mass was observed approximately since 6 p.m. on November 20 until 2 a.m. on November 21, 1998. Dashed lines in Fig. 9 show the behavior of temperature, if there were no specific events and everything was as before. The time interval when the lidar operated is marked in Fig. 9. The time interval when the decrease of temperature was observed is marked as CA (cold air). The area before coming of the cold air and after its going out is marked as WA (warm air).

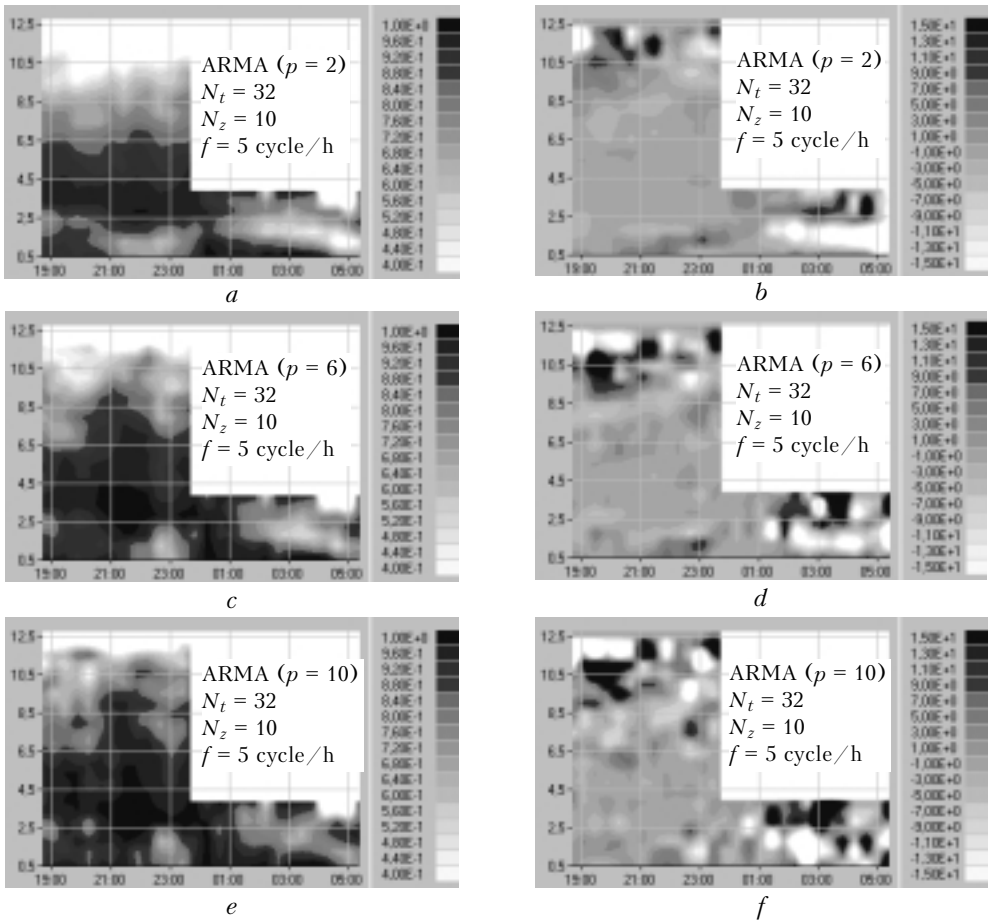


**Fig. 7.** Spatiotemporal maps of the coherency and phase spectra calculated by the ARMA method.

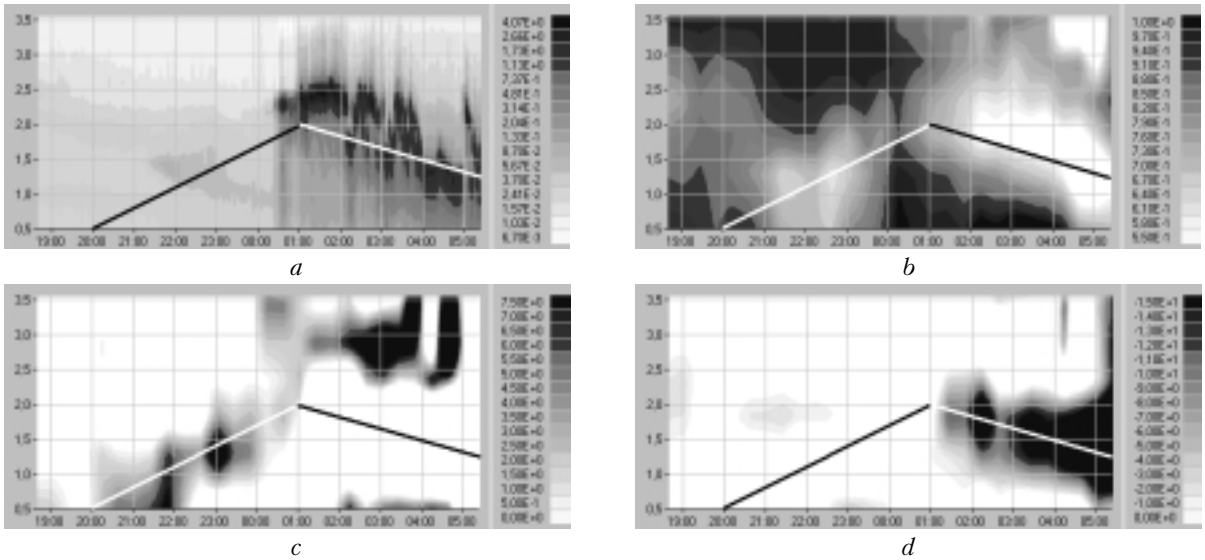


**Fig. 8.** Spatiotemporal maps of the scattering coefficient (*a*) coherency spectra (*b*), positive (*c*) and negative (*d*) phase values. The data were obtained on November 20–21, 1998.

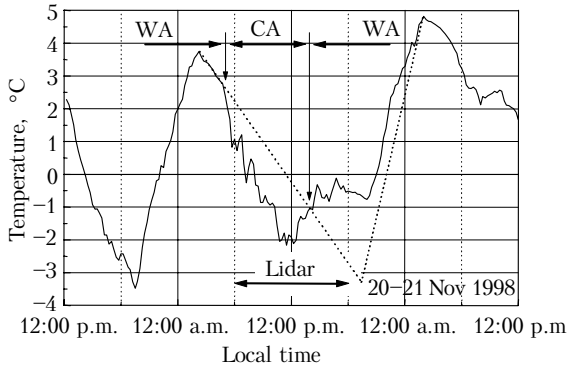


**Fig. 9.** Diurnal behavior of temperature near the ground surface near the lidar. November 20–21, 1998, Tajon, Korea.

Cold air is always more heavy than warm one, so it is always in the lower layer. The region of cold air is shown in Fig. 10. Cold air enters as a wedge under the warm air at the boundaries. Big arrow in Fig. 10 shows the direction of the cold air mass motion. The location of the lidar is shown by long vertical arrow. Naturally, the moving cold air displaces warm air upwards, that explains the positive values of the phase spectrum and movement of this region upwards (see Fig. 8). Correspondingly, the cold air mass when going out is accompanied by the negative phase values, because of warm air descended into position of outgoing cold air. The region of down going motion moved downwards (see Fig. 10). Small arrows in Fig. 10 show the direction of the warm air motion as the cold air mass passes.

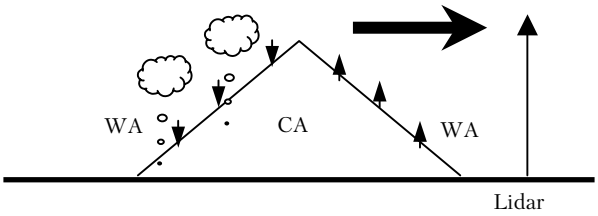


**Fig. 10.** The diagram showing the pass of the cold air mass through the site of lidar observations.

Clouds presented at the back front of the cold air mass are also shown in Fig. 10. In this connection, the following fact revealed is interesting. It is seen from the primary lidar data (see Fig. 8*a*) that the change of the cloud height after 1 a.m. seems to correlate with the data on the phase spectrum in Fig. 8*d*. But, at the same time, no correlation is observed before 1 a.m. when the phase has been positive and the region of positive phase has elevated. It follows from this important fact that the spectral parametric analysis makes it possible to obtain additional, otherwise "hidden" information about the processes occurring in the atmosphere.

Let us consider the coherency spectrum in Fig. 8*b*. It is seen that the coherence spectrum has low values at the boundary of the cold air mass. This area was revealed as a light stripe, which first was directed upwards, and then downwards. The explanation is simple. Warm air is always above the cold air at the boundary. That means, that there is a temperature inversion. As known,[16] the Archimedes force at temperature inversion is negative, and so it prevents the turbulent exchange between neighboring layers (see Fig. 1). It explains why the coherency spectrum has low values and was an indicator of the regions, in which turbulent exchange between the neighboring layers is difficult.

## Conclusion

Thus, we have illustrated how the statistical processing of lidar data can become useful. The fact is obvious for us, that the parametric approach is more versatile and has more possibilities in comparison with the traditional classic Fourier analysis. Statistical processing and use of the coherency and phase spectra extends the list of parameters that can be calculated based on the lidar data.

It has been shown that the use of the ARMA model makes it possible to obtain the estimates of auto- and cross-spectra with higher frequency resolution and with the accuracy not worse than the non-parametric approach provides. One should choose the order of the ARMA model based on the problem to be solved, but in any case, it is useful to start the statistical processing of lidar data with low values of the order of the model $p$.

Spatial and temporal scales of the cold air mass passing over the observation site have been estimated by means of the spectral parametric processing of the data obtained by the aerosol MPL lidar. The coherence spectrum has served as an indicator of the position of the boundary of the temperature inversion. The phase spectrum has unambiguously shown the direction of the slow vertical movement of the aerosol inhomogeneities.

Let us note that one can estimate the velocity values[13] from the phase values, but it is out of the frameworks of this paper. The ways for applying the statistical ARMA model to analysis of the lidar data can be different and depend on the problem stated and inventiveness of researchers.

### Acknowledgments

Authors would like to thank Prof. G.N. Glazov for a number of valuable advices and the advanced idea of using the parametric approach for analysis of the data of lidar sounding.

### References

1. E.W. Eloranta et al., J. Appl. Meteorol. **19**, 598–605 (1980).
2. N. Sugimoto et al., Jpn. J. Appl. Phys. **37**, 5598–5603 (1998).
3. Yu.S. Balin, I.A. Razenkov, and A.P. Rostov, Atmos. Oceanic Opt. **7**, No. 7, 513–516 (1994).

4. R.K. Otnes and L. Enochson, *Applied Time Series Analysis* (John Wiley & Sons, 1978), 428 pp.
5. J.S. Bendat and A.G. Piersol, *Engineering Applications of Correlation and Spectral Analysis* (John Wiley & Sons, 1980), 310 pp.
6. J. Van der Hoven, J. Meteorol. **14**, No. 2, 160–164 (1957).
7. L.T. Matveev, *Course of General Meteorology* (Gidrometeoizdat, Leningrad, 1976), 639 pp.
8. S.L. Marple, *Digital Spectral Analysis with Applications* (Prentice-Hal, Inc., 1988), 582 pp.
9. A.S. Monin and A.M. Yaglom, *Statistical Hydromechanics* (Nauka, Moscow, 1965), Part 1, 640 pp.
10. T.T.M. Nieuwstadt and H.D. Van Dop, eds., *Atmospheric Turbulence and Air Pollution Modeling* (Reidel Publishing Company, 1981), 351 p.
11. A.H. Nuttall, "*Multivatiate linear predictive spectral analysis employing weighted forward and backward averaging: a generation of Burg's algorithm,*" Naval Underwater Systems Center Technical Report No. 5501, New London, Conn. (1976).
12. O.N. Strand, IEEE Trans. Autom. Control. **AC-22**, 634–640 (1977).
13. I.A. Razenkov, H.K. Cha, D.H. Kim, and J.M. Lee, Proceedings of SPIE **3983**, 299–305 (1999).
14. J.D. Spinhirne, IEEE Trans. Geo. Rem. Sens. **31**, 48–55 (1993).
15. J.D. Klett, Appl. Opt. **24**, No. 11, 1638–1643 (1985).
16. R.B. Stull, *An Introduction to Boundary Layer Meteorology* (*Atmospheric Sciences Library*, Vol. 13) (Kluwer Academic Publishers, Netherlands)